



Linkages Between Tropical Cyclones and Extreme Precipitation over China and the Role of ENSO

Licheng Wang¹ · Zhengnan Yang¹ · Xihui Gu² · Jianfeng Li³

Published online: 30 June 2020
© The Author(s) 2020

Abstract This research investigated the linkages between tropical cyclones (TCs) and extreme precipitation, and their associations with El Niño-Southern Oscillation (ENSO) over China. The contribution of TC-induced to total extreme precipitation events along the southeast coast of China was higher than 50%, and the values gradually decreased as TCs moved inland. However, the precipitation extremes (magnitude and frequency) related to TCs did not show statistically significant changes over the most recent 57 years. The impacts of TCs on precipitation extremes are evidently modulated by the ENSO phases. We found less extreme precipitation linked with TCs in southeastern China during El Niño phase, because of the fewer TC tracks over this region and less TC genesis in the western North Pacific (WNP). The small TC track density over southeastern China is due to the prevalent westerly steering flow and abnormal integrated vapor transport from northern to southern China during El Niño years. Additionally, warmer sea surface temperature, more vigorous westerlies, larger vorticity in 250 hPa, and higher divergence in 850 hPa in an El Niño phase jointly displaced the mean genesis of the WNP TCs eastward and this led to fewer TCs passing through southeastern China.

Keywords China · ENSO (El Niño-Southern Oscillation) · Extreme precipitation · Large-scale environmental variables · Tropical cyclones

1 Introduction

The disasters caused by tropical cyclones (TCs) are usually very severe and the accompanying property losses are huge (Zhang et al. 2009; Mumby et al. 2011; Peduzzi et al. 2012). Frequency and intensity of TCs, the two major features that are highly related to TC-induced losses, have been reported to increase in all TC basins (Webster et al. 2005). Yet TCs can be beneficial by mitigating soil moisture drying (Gu et al. 2019a). Global warming is an important contributor to the rise in the occurrence rate of high-intensity TCs (Mendelsohn et al. 2012). A large part of TCs around the world is generated in the western North Pacific (WNP), and TCs that originate from this region frequently attack eastern China, a region with booming socioeconomic development and the highest population density in the world (Zhang et al. 2009). Recently, China has been plagued by super typhoons that occur in the WNP, such as Mangkhut (ID: 1822, in 2018) that killed five people and led to economic losses of CNY 5.2 billion Yuan. These damage losses are mostly caused by flash flooding triggered by precipitation extremes associated with TCs (Jonkman et al. 2009; Zhang, Gu et al. 2018). Therefore, investigating the linkages between TCs and extreme precipitation is crucial to understanding and mitigating TC-induced damages and losses.

Many studies have concentrated on the relationships between extreme precipitation events and TCs (Shepherd et al. 2007; Khouakhi et al. 2017; Zhang, Lai et al. 2018).

✉ Xihui Gu
guxihui421@163.com

¹ Department of Atmospheric Science, School of Environmental Studies, China University of Geosciences, Wuhan 430074, China

² State Key Laboratory of Simulation and Regulation of Water Cycle in River Basin, China Institute of Water Resources and Hydropower Research, Beijing 100038, China

³ Department of Geography, Hong Kong Baptist University, Hong Kong, China

The contributions of TCs to annual maximum (AM) daily precipitation have been estimated over various regions, such as 40–50% in northwestern Australia (Khouakhi et al. 2017), more than 30% in the east coast of the United States (Aryal et al. 2018), 20–30% along the coast of the Gulf of Mexico and 40–65% in southeastern Japan (Khouakhi et al. 2017), and 35–60% along the southeastern coast of China (Khouakhi et al. 2017; Zhang, Lai et al. 2018). Most of these studies linked TCs with AM 1-day precipitation. However, the AM precipitation, defined as the largest daily precipitation occurring over the course of a year, cannot capture all the TC-induced precipitation extremes (Gu et al. 2020). The AM captures one event in a year while the peak-over-threshold (POT) can capture multiple events that are smaller than the AM (Villarini et al. 2013). Generally speaking, heavy precipitation is defined as the number of days exceeding a selected threshold value that is counted for every year through a POT method (Villarini et al. 2013). Based on previous studies, POT sampling method that can break the limitation of AM sampling is used to obtain the magnitude and frequency of TC-induced extreme precipitation, and POTs show a much stronger signal of precipitation extremes (Gu et al. 2017b; Khouakhi et al. 2017).

Climate oscillations defined by sea surface temperature (SST) anomalies—such as El Niño-Southern Oscillation (ENSO)—have a remarkable effect on TC activity and they regulate TC-induced extreme precipitation (Wang and Chan 2002; Villarini et al. 2014; Corporal-Lodangco et al. 2016). In general, ENSO has a strong influence on the variations in TC geneses, intensity, lifetime, and track in the WNP (Camargo and Sobel 2005; Wang et al. 2015). For example, the air flow on the western side of the WNP is abnormally depressed, inhibiting the TC formation and translation during El Niño phases (Chan 2000). Accumulated cyclone energy over the sea adjoining southeastern China is much lower during El Niño phases than during La Niña phases (Corporal-Lodangco et al. 2016). Moreover, the amount of the WNP TCs recurving northward of 35°N is twofold in warmer years (Wang and Chan 2002).

There exists an extensive literature that studies the impacts of ENSO on WNP TCs as well as extreme precipitation (Wu et al. 2003; Chan and Zhou 2005; Zhang et al. 2016; Gu et al. 2017b), but the possible mechanisms behind the impacts of ENSO on TC-induced precipitation extremes are still unclear. Khouakhi et al. (2017) explored the connection between ENSO and TC-induced extreme precipitation, whereas the observed daily precipitation dataset, which is provided by the GHCN (Global Historical Climatology Network), is subjected to a short temporal length (~ 25 years), low quality (for example, a sizable amount of missing value), and sparse sites (several hundreds) for China. Zhang, Gu et al. (2018) assessed the

dependence of TC-induced extreme precipitation on different ENSO phases because of the close connection between TC genesis and ENSO; overall, the physical mechanisms behind the modulation of ENSO on the connection between extreme precipitation and TCs are not yet well explored.

Although previous studies have examined the relationship between extreme precipitation and TCs, these studies were mostly based on the AM extreme precipitation, suffered from deficient observations, and lacked physical mechanism analysis. In this study, we first calculated the contributions of TCs to precipitation extremes (such as magnitude defined by AM sampling and frequency defined by POT sampling) based on long-term records, and then explored how ENSO influences TC-induced precipitation extremes. Our objectives were to answer: (1) whether these contributions are sensitive with the durations in magnitude (that is, the maximum n -day precipitation) and the thresholds in frequency (that is, the exceeding days over n -th of records); and (2) whether there is any pattern of ENSO impact on extreme precipitation induced by TCs; and if so (3) what the possible reasons are behind the pattern.

2 Data

In this section, we briefly introduce the datasets used in this study. Observed daily precipitation data were used to extract the precipitation extremes, and TC best tracks were employed to identify the relationship between TCs and precipitation extremes. Niño 3.4 index data were used to examine the relationship between ENSO and TC-induced extreme precipitation, and the possible mechanisms behind this relationship were explored by analyzing the changes in large-scale environmental variables from the NCEP-NCAR (National Centers for Environmental Prediction-National Center for Atmospheric Research).

2.1 Observed Daily Precipitation and TC Best Tracks

We collected in-site daily precipitation records from 2474 stations over China from the China Meteorological Information Center¹ (Ma et al. 2015; Gu et al. 2019b). The precipitation records span the period from 1951 to 2016, and most stations have a record length greater than 55 years (Fig. 1). The period 1960–2016 was selected for our analysis, and a station was rejected if the missing values are more than 5% in this period. In the selected 1937 stations, 92% have missing data of less than 1%. We used

¹ <http://data.cma.cn/>.

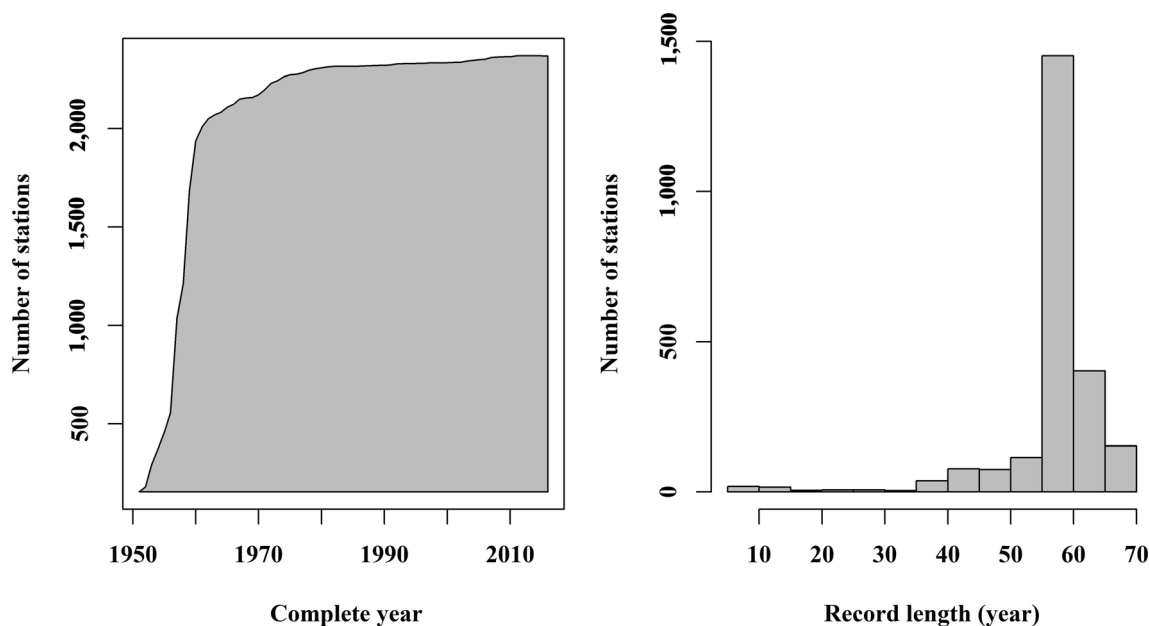


Fig. 1 Precipitation observations in terms of **a** the number of weather stations with complete records for a given year; and **b** the number of stations with different record lengths of daily precipitation data

the gap-filling method to fill the missing value. A missing value of a single day was filled by the mean of rainfall of nearby stations. Missing values of two consecutive days or more were filled by the long-term means of the same days in other years. According to a previous study (Zhang et al. 2011), this method did not affect the results significantly.

The global TC track information was extracted from the IBTrACS (International Best Track Archive for Climate Stewardship),² including latitude and longitude of the center of each TC in each six hours (Knapp et al. 2010). In this research the IBTrACS data for the WNP during 1960–2016 were selected to analyze the impacts of TCs, and the intensity of TCs was classified according to the Saffir-Simpson hurricane intensity scale (Khouakhi et al. 2017) (Fig. 2).

2.2 ENSO Phases and NCEP-NCAR Reanalysis Dataset

The SST anomalies in the region between 5°CN–5°CS and 170–120°CW were used to derive ENSO phases. We collected monthly Niño 3.4 index data from the Global Climate Observing System–Working Group on Surface Pressure (GCOS-WGSP).³ Most of the WNP TCs occurred in May–November (Lee et al. 2010); thus seasonal means of the Niño3.4 index were calculated—for May–July (MJJ), June–August (JJA), July–September (JAS), August–

October (ASO), and September–November (SON). Following Lyon and Camargo (2009), we divided the Niño 3.4 index during the 57-year period into three groups: (1) El Niño years, 5 month running average of the Niño 3.4 index > 0.5 °C; (2) neutral years, the mean of the Niño 3.4 index > -0.5 °C and < 0.5 °C; and (3) La Niña years, the mean of the Niño 3.4 index < -0.5 °C.

Monthly SST, meridional and zonal wind speed, specific humidity, vorticity, and divergence data during the period 1948–2016 with $2.5^\circ \times 2.5^\circ$ spatial resolution were collected from NCEP-NCAR.⁴

3 Methodology

In this section, we first introduce how to identify whether an extreme precipitation event was induced by a TC. Then, we describe the equations of the two methods—the logistic and Poisson regressions that were used to quantify the relationship between TC-induced extreme precipitation and ENSO phases. Finally, the definitions of steering flow and integrated vapor transport are presented.

3.1 Identification of TC-Induced Extreme Precipitation

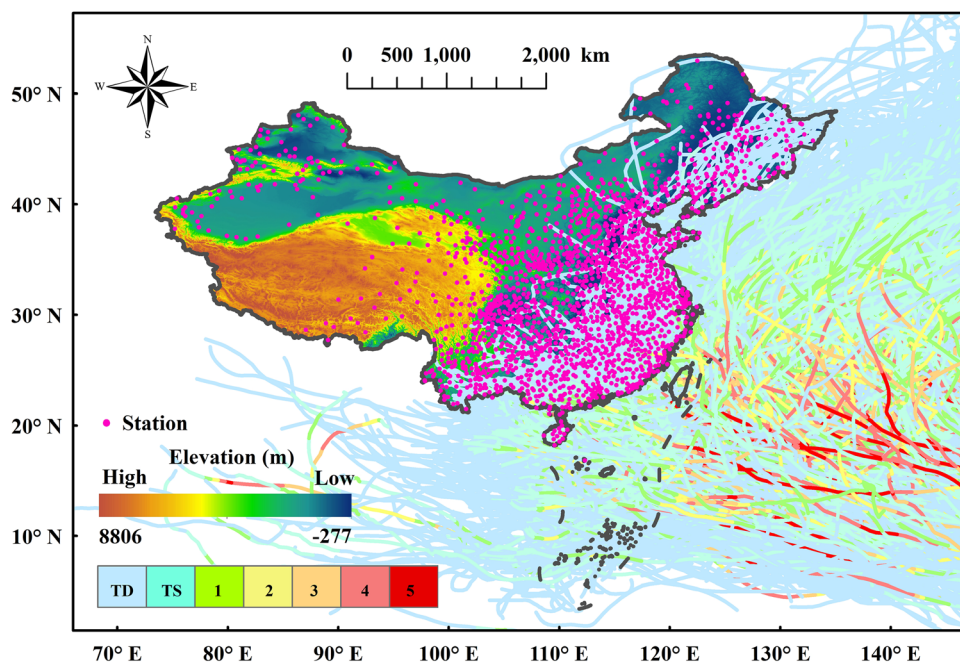
In this study, we examined the contribution of TCs to extreme precipitation through the methods of annual maximum (AM) and peak-over-threshold (POT). In AM

² <https://www.ncdc.noaa.gov/ibtracs/>.

³ https://psl.noaa.gov/gcos_wgsp/Timeseries/Data/nino34.long.anom.data.

⁴ <https://psl.noaa.gov/data/gridded/data.ncep.reanalysis.html>.

Fig. 2 Geographic locations of the selected 1937 weather stations (pink dots), the observed tropical cyclone (TC) tracks from 1960 to 2016 (colored lines), and the digital elevation model in China. The intensities of TCs are classified based on the Saffir-Simpson hurricane intensity scale



sampling, the total amount of annual maximum n -days precipitation was taken as the magnitude; and in POT sampling, the number of days in each year in excess of a threshold was taken as the frequency (Villarini and Denniston 2016; Gu et al. 2017a, c; Aryal et al. 2018). Considering that TC-induced extreme precipitation may persist for several days, the AM precipitation occurring in an n -day ($n = 1, 2, \text{ and } 3$) window for each site was extracted from daily precipitation. Moreover, different thresholds—the 90th, 95th, and 99th percentile of non-zero rainfall—in the POT sampling were used to evaluate if the contributions of TCs are sensitive to the frequency of extreme precipitation (Krishnamurthy et al. 2016).

It is common to identify TC-induced extreme precipitation using radius-depend circle that represents the range of precipitation associated with a TC (Jiang and Zipser 2010; Lee et al. 2010). Although the employed radiuses vary from 250 km to 1000 km (Chen et al. 2010), most studies agree that the radius usually used should be 500 km (Smith et al. 2011; Gu et al. 2017c; Khouakhi et al. 2017). Thus if a daily precipitation is to be identified as induced by a TC, two criteria should be satisfied: (1) the distance between TC storm center and precipitation station is less than 500 km; and (2) the difference between the date of TC tracks and occurrence time of extreme precipitation is within ± 1 day (Knight and Davis 2009; Zhang, Gu et al. 2018).

3.2 Logistic and Poisson Regressions

Whether TC-induced AM precipitation tends to occur in a La Niña or El Niño phase can be assessed by the probability estimated in the logistic regression model (Khouakhi

and Villarini 2017). Specifically, whether an AM precipitation event is associated with a TC or not can be assigned a value of 1 or 0; thus the relationship between the binary response variable and ENSO values can be described as follows (Villarini and Denniston 2016; Aryal et al. 2018):

$$\log\left(\frac{\pi}{1 - \pi}\right) = \beta_0 + \beta_1 x \tag{1}$$

where π is the occurrence probability of a AM precipitation event induced by TCs; β_0 is the intercept and β_1 is the slope; x is the seasonal averaged ENSO values defined in Sect. 2.2. If β_1 is more (less) than zero, there is a larger probability of TC-induced AM precipitation event occurring in an El Niño (La Niña) phase. The p value is used to evaluate if the probability reaches 0.05 significance level or not. Only the stations with at least five TC-induced AM precipitation events were selected to be fitted by the logistic regression model.

Poisson regression was employed to examine the dependence of the frequency of extreme precipitation events caused by TCs on ENSO states. The number of days exceeding the threshold and associated with TCs in each year can be simulated by a point process that follows Poisson distribution (Villarini et al. 2013; Villarini and Denniston 2016; Aryal et al. 2018):

$$P(N_i = k | \lambda_i) = \frac{e^{-\lambda_i} \lambda_i^k}{k!} \quad (k = 0, 1, \dots) \tag{2}$$

where N_i is the number of TC-induced extreme precipitation in year i ; the occurrence rate for TC-induced extreme precipitation, λ_i , is a non-negative

variable, and can be modeled by exponential function (Villarini and Denniston 2016; Aryal et al. 2018):

$$\lambda_i = \exp(\beta_0 + \beta_1 x_i) \quad (3)$$

where the meanings of β_0 , β_1 , and x are the same as those in the logistic regression. β_1 is more (less) than zero, suggesting that larger (smaller) numbers of TC-induced extreme precipitation days are more likely to happen in an El Niño (La Niña) phase. The p value is used to evaluate if the relationship reaches the 0.05 significance level or not.

3.3 Dynamics of the Role Played by ENSO

To explain the results of the logistic regression model and the Poisson regression model with the related dynamic processes, we calculated the steering flow and integrated vapor transport. Wind fields from 850 to 300 hPa were pressure-weighted, averaged, and then were taken as steering flow (unit: m/s), which has a large influence on TC tracks (George and Gray 1976; Chan and Gray 1982; Aryal et al. 2018). The transported total amount of water vapor (IVT) integrates specific humidity, U wind, and V wind by atmospheric levels (Nayak et al. 2016; Aryal et al. 2018):

$$IVT = \sqrt{\left(\frac{1}{g} \int_{\text{surface}}^{300} qudp\right)^2 + \left(\frac{1}{g} \int_{\text{surface}}^{300} qvdp\right)^2} \quad (4)$$

where q , u , and v are specific humidity (kg/kg), and U and V wind (m/s), respectively; g is the gravity acceleration (m/s^2), and p is pressure.

4 Results and Discussion

In this section, we first investigate the linkages between TCs and extreme precipitation, including the contributions of TCs to the magnitude and frequency of extreme precipitation and the long-term trends in the magnitude and frequency of TC-induced extreme precipitation over China. Second, we employ the logistic and Poisson regressions to quantify the relationships between the magnitude and frequency of TC-induced extreme precipitation and ENSO phases, respectively. Finally, the behaviors of TC track density and genesis, steering flow, moisture flux, and large-scale environmental variables during three ENSO phases (that is, La Niña phase, neutral phase, and El Niño phase) are analyzed to explore the possible mechanisms behind the relationships.

4.1 Linkages between TCs and Extreme Precipitation

There are 887 out of the 1937 stations experiencing AM and/or POT precipitation events caused by WNP TCs (Figs. 3 and 4). The contributions of TCs to AM and POT precipitation across China exhibited very strong regional features. As the TCs moved inland from southeastern China to northwestern China, the contributions gradually

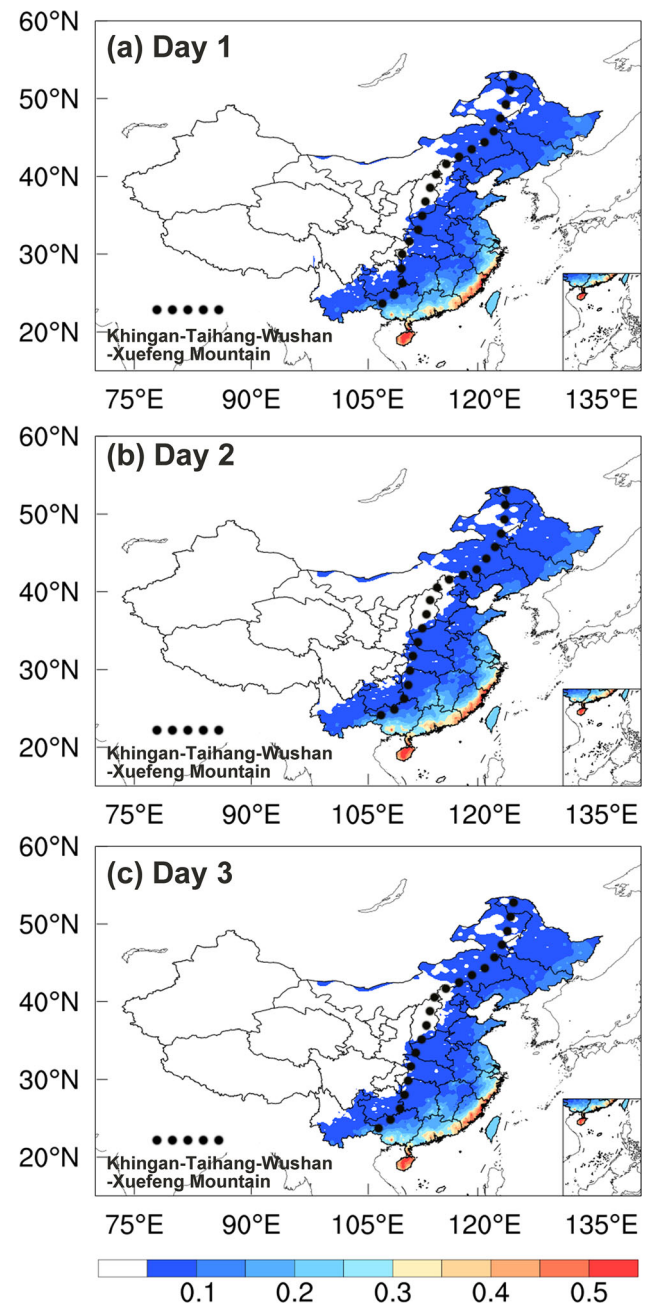


Fig. 3 Contributions of tropical cyclones (TCs) to annual maximum (AM) 1-day (Day 1) (a), 2-day (Day 2) (b), and 3-day (Day 3) (c) precipitation in the mainland of China

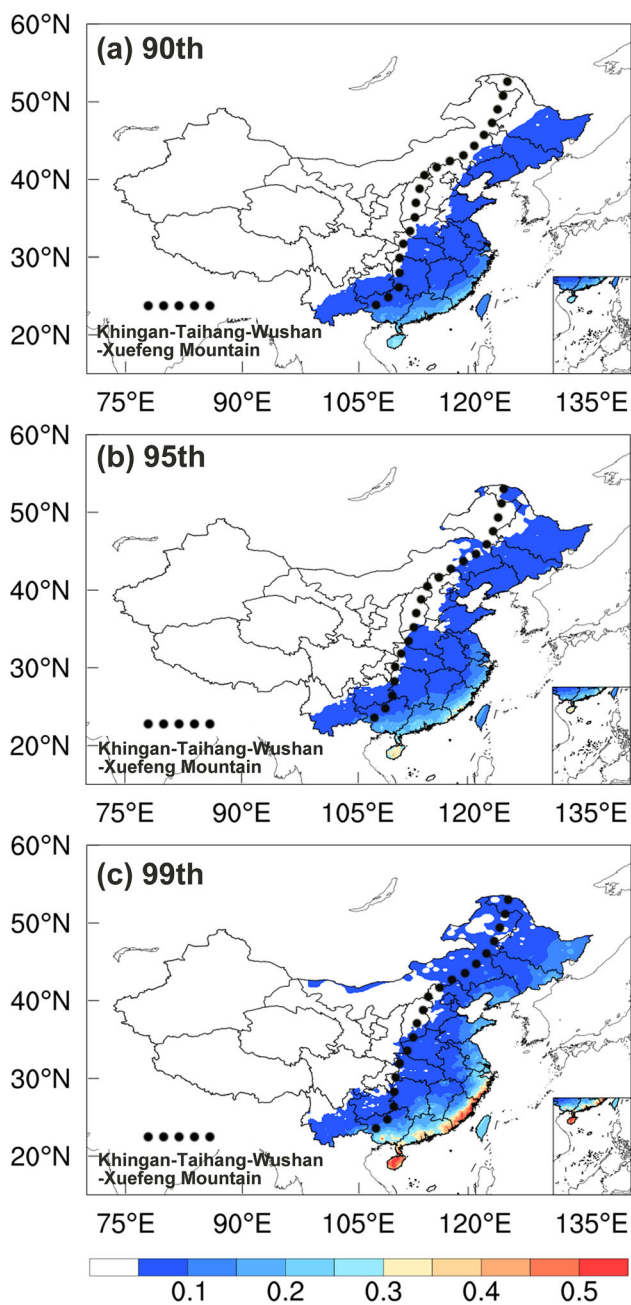


Fig. 4 Contributions of tropical cyclones (TCs) to extreme precipitation obtained by peak-over-threshold (POT) sampling with 90th (a), 95th (b), and 99th (c) percentile of the precipitation distribution as thresholds in the mainland of China

decreased (Jiang and Qi 2016). The coastal areas in southeastern China, which are the regions with the highest level of economic development and population density in China, are characterized by the highest contributions (that is, more than 50% in at least 70 stations, Fig. 3). The stations with contributions ranging from 20 to 50% (at least 236 stations) are located in southeastern China where precipitation extremes are not only triggered by TCs, but also warm season convective systems and extratropical

systems in spring (Vellore et al. 2016; Zhou et al. 2006). Although the regions with precipitation extremes induced by TCs even go northward to northeastern China, the contributions in these regions were less than 15% (Fig. 3). Except for the TC-induced extreme precipitation in northern and northeastern China, more than 80% of precipitation extremes were triggered by organized warm season convective systems (Gu et al. 2017c). There is a high similarity in the spatial patterns of these contributions in different durations (that is, the AM 1-day, 2-day, and 3-day precipitation).

It should be noted that a few of the stations in central China (25–35°W, 110–115°E) showed a weak linkage between precipitation extremes and TCs (contributions less than 10%, Fig. 3). However, TC-induced damages in this region could also be severe. For example, in this region, Typhoon Nina in 1975 induced a rare storm with the amount of maximum 6 h precipitation equal to the current world record of 840 mm. This storm event directly caused 26,000 deaths and impacted about 10 million people (Teegavarapu 2013; Yang et al. 2017). The forward path of TCs is prevented by the undulating mountains (that is, the Great Khingan-Taihang-Wushan-Xuefeng Mountain, which is also the dividing line between the first and the second topographic steps in China) that naturally draw a divided line and shield western China (Ren et al. 2007) (Figs. 1 and 3).

The areas affected by TCs slightly expand along with the POT precipitation in higher thresholds (Fig. 4). Specifically, the numbers of stations with more than 5% of POT precipitation induced by TCs are 597 for 90th, 691 for 95th, and 845 for 99th. The contributions in POT precipitation with the three thresholds exhibited discrepancies in the coastal areas of southeastern China. In these areas, the contributions of TCs increased from 30% to more than 50% in extreme precipitation defined by thresholds from 95th to 99th. This indicates that the contributions of TCs to POT precipitation heavily depend on the threshold selected in POT sampling. The contributions of TCs to AM precipitation are higher compared to the POT precipitation (Fig. 4). The spatial distributions and the values of the contributions are most likely resemble precipitation levels that occur between AM precipitation and POT precipitation in the 99th threshold. These results indicate that TCs may be a larger cause of these upper-tail precipitation extremes than other local precipitation mechanisms (Ren et al. 2006).

The contributions in our study are generally in agreement with the existing literature (Ren et al. 2006; Chang et al. 2012). Chang et al. (2012) reported that the percentage of TC-induced precipitation extremes over the southeastern coast is 50–70%. Yin et al. (2010) showed clearly that the ratio between TC-induced severe rain days and the total amounts to more than 50% in Fujian Province

in southeastern China. Ren et al. (2006) revealed that the amount of TC-induced extreme precipitation can be more than 500 mm/year in most parts of the southeastern coast of China. Chang et al. (2012) found northern and northeastern China experienced larger influences of TCs (20–35% of precipitation extremes caused by TCs) than in our study (about 10–15%), probably due to different definitions of TC-induced precipitation, record lengths, and network densities.

In addition to the contributions of TCs, we also employed the Mann–Kendall test (Mann 1945; Kendall 1975) and Poisson regression (Villarini et al. 2013) to detect the trends in extreme precipitation (that is, magnitude and frequency) caused by TCs (Figs. 5 and 6). Although some stations show significant increases or decreases in extreme precipitation caused by TCs, the signal that most stations indicate reveals significant temporal change is not strong (Figs. 5 and 6). It is also worth pointing out that the magnitude of TC-induced extreme precipitation tends to increase in southeastern China, while the frequency of TC-induced POT precipitation tends to decrease in this region (Figs. 5 and 6). This result is in agreement with Chang et al. (2012). Over the period 1975–2009, the annual mean overland duration of TCs has increased significantly over China (Chen et al. 2011). The increasing lifetime of TCs may be offset by the decrease in the number of TCs affecting China (Ren et al. 2006), which may lead to the stationary influence of TCs on precipitation extremes in the long term.

4.2 Relationships Between TC-Induced Extreme Precipitation and ENSO

Figures 7 and 8 show the relationships between TC-induced extreme precipitation and ENSO. First, logistic regression was employed to investigate the occurrence likelihood of TC-induced AM precipitation in different ENSO phases by the estimated β_1 coefficient and its p value (Fig. 7). The number of stations with positive β_1 coefficient is almost equal to that with negative β_1 coefficient (around 650). However, the β_1 coefficient at different levels of significance shows an evident spatial pattern. Most of the stations with positive β_1 coefficient are located in northern and northeastern China, implying that TCs are more likely to produce more AM precipitation event in El Niño years in this region. There is a higher likelihood of TC-induced AM precipitation occurring in La Niña phase over southeastern China where the β_1 coefficient is less than zero. Similar conclusions are valid for the AM extreme precipitation with different durations and for the ENSO values from different seasons.

The Poisson regression method was employed to explore the relationship between the frequency of TC-induced POT precipitation and ENSO, which is similar to the

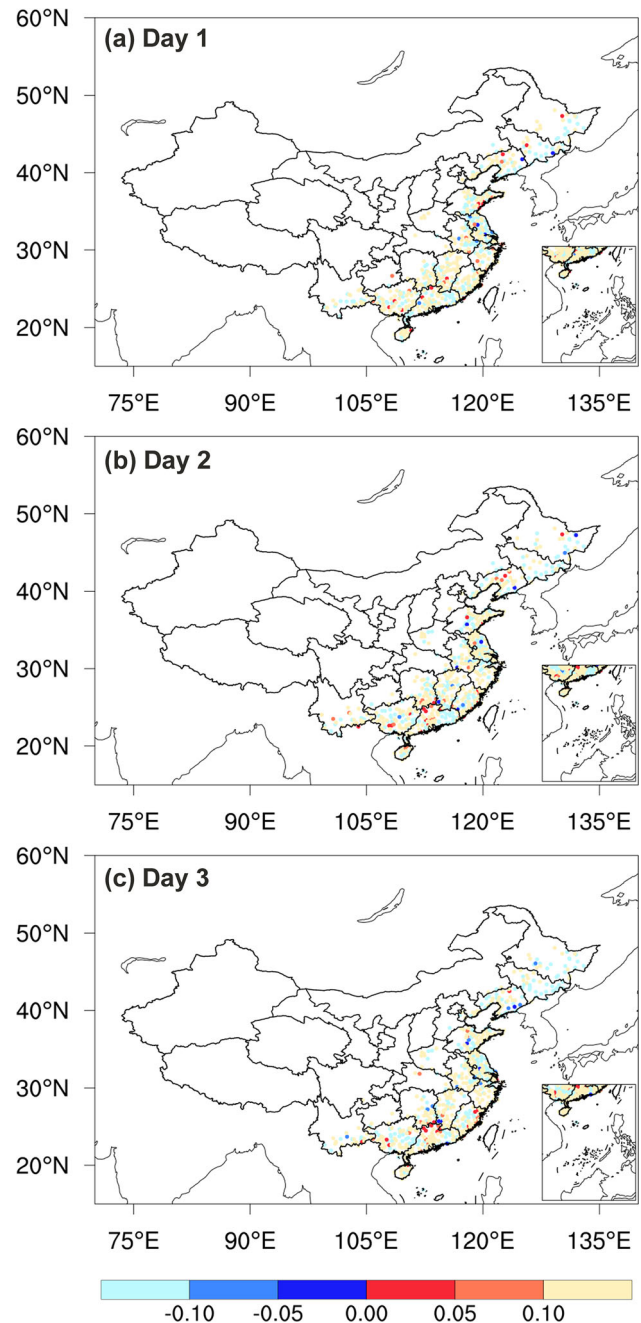


Fig. 5 Spatial distributions of trends in tropical cyclone (TC)-induced annual maximum (AM) Day 1 (a), Day 2 (b), and Day 3 (c) precipitation in the mainland of China. The trends were detected by the Mann–Kendall method and the values in each panel indicate the corresponding significance p values. The red (blue) p values indicate positive (negative) trends in TC-induced AM precipitation

logistic regression (Fig. 8). The results for the frequency of these events are highly consistent with that for AM precipitation from the logistic regression. The signal that higher (lower) possibility of TC-induced events takes place in La Niña (El Niño) phase in southeastern China (northern and northeastern China) is stronger when we examine POT

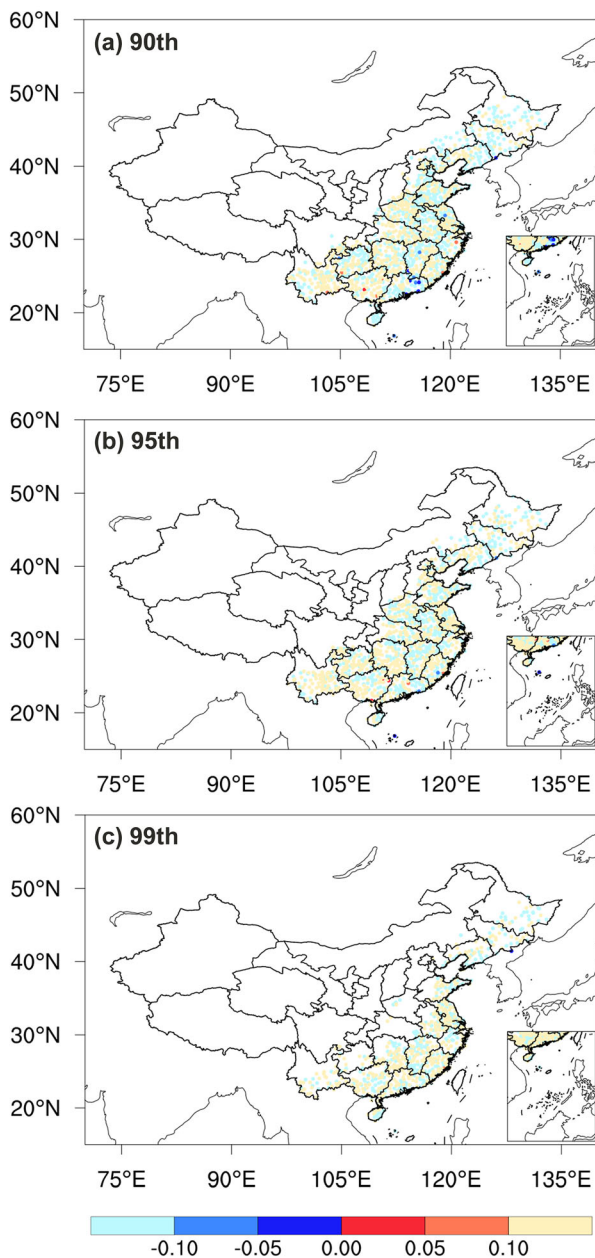


Fig. 6 Spatial distributions of trends in tropical cyclone (TC)-induced extreme precipitation obtained by peak-over-threshold (POT) sampling with 90th (a), 95th (b), and 99th (c) percentiles in the mainland of China. The trends were detected by the Poisson regression method and the values in each panel indicate the corresponding significance p values. The red (blue) p values indicate positive (negative) trends in TC-induced POT extreme precipitation

events. For example, the number of stations with significant coefficients (at the 0.05 significance level) is 34 for AM 1-day precipitation during SON season (Fig. 7m), while the number is 176 for POT precipitation (Fig. 8m). The signal is stronger for the SON ENSO values than the MJJ values, implying the averages of SON Niño 3.4 values is a better predictor for TC-induced extreme precipitation

than other seasonal values. Overall, ENSO is a strong signal that can modulate the TC-induced extreme precipitation because of the coherent spatial patterns between AM and POT events and stable linkages among different seasonal ENSO values.

Generally speaking, our findings are in keeping with the existing literature (Khouakhi et al. 2017; Zhang, Gu et al. 2018). Khouakhi et al. (2017), which concluded that TC-driven extreme precipitation tends to occur more in southeastern China during La Niña years from a global analysis. These regional features between ENSO and TC-induced extreme precipitation depend on the responses of TC tracks to ENSO phases. Previous studies have shown clearly that the intensity and duration of TCs are likely to be stronger and longer over the WNP during El Niño years, and the trajectories of these TCs are likely to be more northward recurved (Wang and Chan 2002; Camargo and Sobel 2005; Corporal-Lodangco et al. 2016), which helps to trigger the extreme precipitation over northern and northeastern China.

4.3 Possible Mechanisms Behind the Relationship

Here we further explore the possible mechanisms behind the relationship revealed by the logistic regression and the Poisson regression. We calculated the meteorological factor between May and November in which the activities of tropical cyclones mainly concentrated during 1960–2016. The differences in the likelihood of TC-induced extreme precipitation occurring in different ENSO phrases are related to the variability in TC track density (Fig. 9). During the neutral phase, the anomalies of TC track density over southeastern China and the South China Sea are negative (Fig. 9b). When the neutral phase turned into an El Niño phase, the negative anomalies of TC track density in the same region became more obvious and stronger (Fig. 9c). On the other hand, we also observed weak positive density anomalies in the Yellow Sea (adjoining North China) during the La Niña phase, although the strong negative TC track density anomalies over the WNP were legible (Fig. 9a). ENSO also impacts on the likelihood of TC-induced extreme precipitation through moisture transport. The integrated vapor transport features a path from the South China Sea to northern China during the La Niña years, which is also favorable for a greater amount of precipitation triggered by TCs (Fig. 9a). Additionally, the integrated vapor transport is abnormally transited from north to south China during the El Niño years, which blocks the warm-wet moisture originated from the WNP and then the moisture flux is not sufficient to produce more TC-induced extreme precipitation (Fig. 9c). Overall, the spatial patterns of TC track density anomalies during different phases of ENSO are in line with that of the

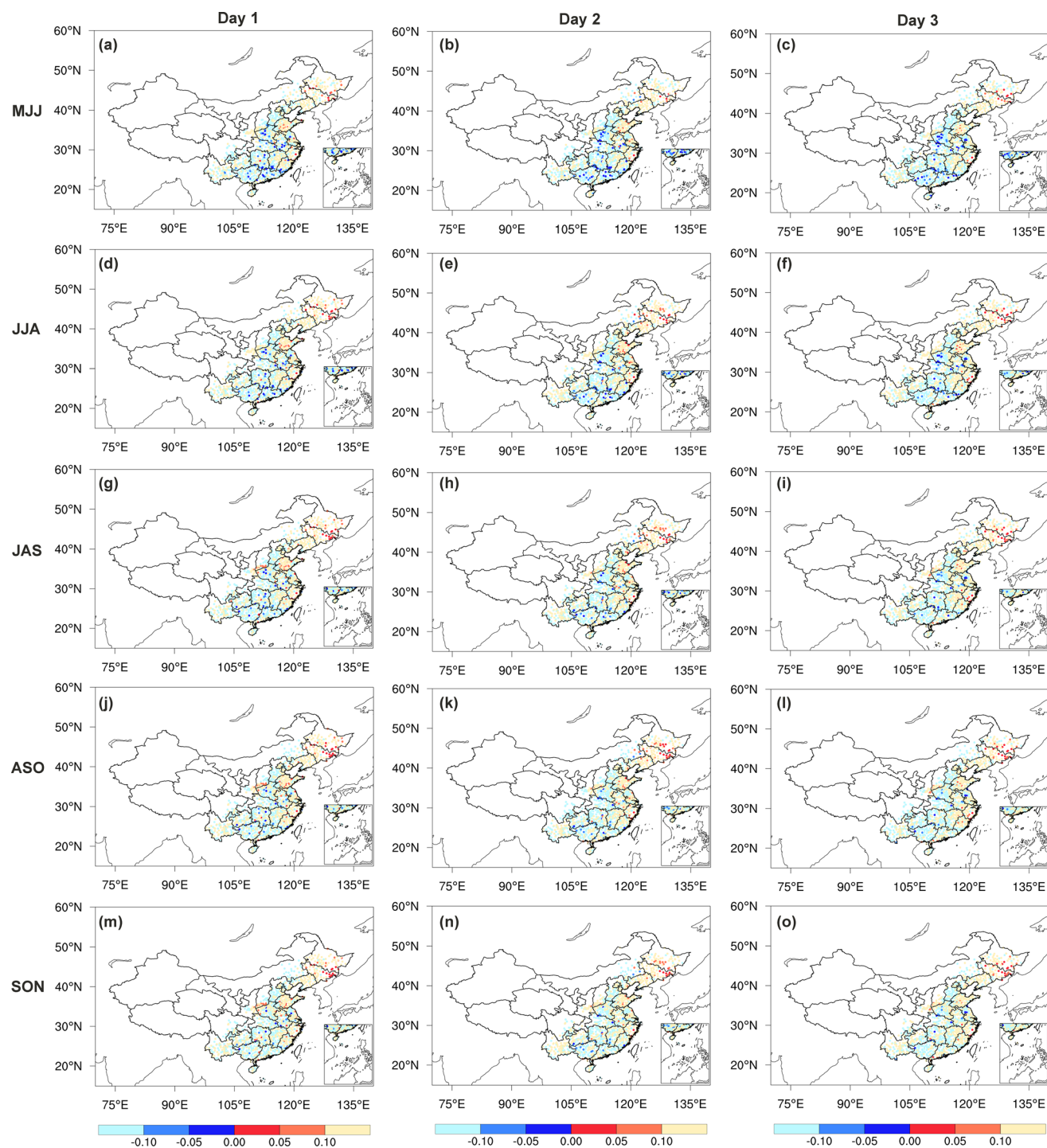


Fig. 7 Relationship between the tropical cyclone (TC)-induced annual maximum (AM) Day 1, Day 2, Day 3 precipitation and seasonal Niño-3.4 values in the mainland of China. The relationship was identified based on logistic regression, and the color bars are p values of the β_1 coefficients. Negative p values (blue circles) represent that the β_1 coefficients are less than zero, indicating a

relationship between ENSO and TC-induced extreme precipitation.

greater probability of TC-induced AM precipitation during La Niña years, and positive p values (red circles) indicate a greater probability during El Niño years. The monthly Niño-3.4 values were averaged for each TC season: May–July (MJJ); June–August (JJA); July–September (JAS); August–October (ASO); and September–November (SON)

Further, the density of TC tracks is associated with two factors: TC genesis and steering flow (Fig. 10). The low TC genesis density (specifically, 120°–150°E, 15°–30°W)

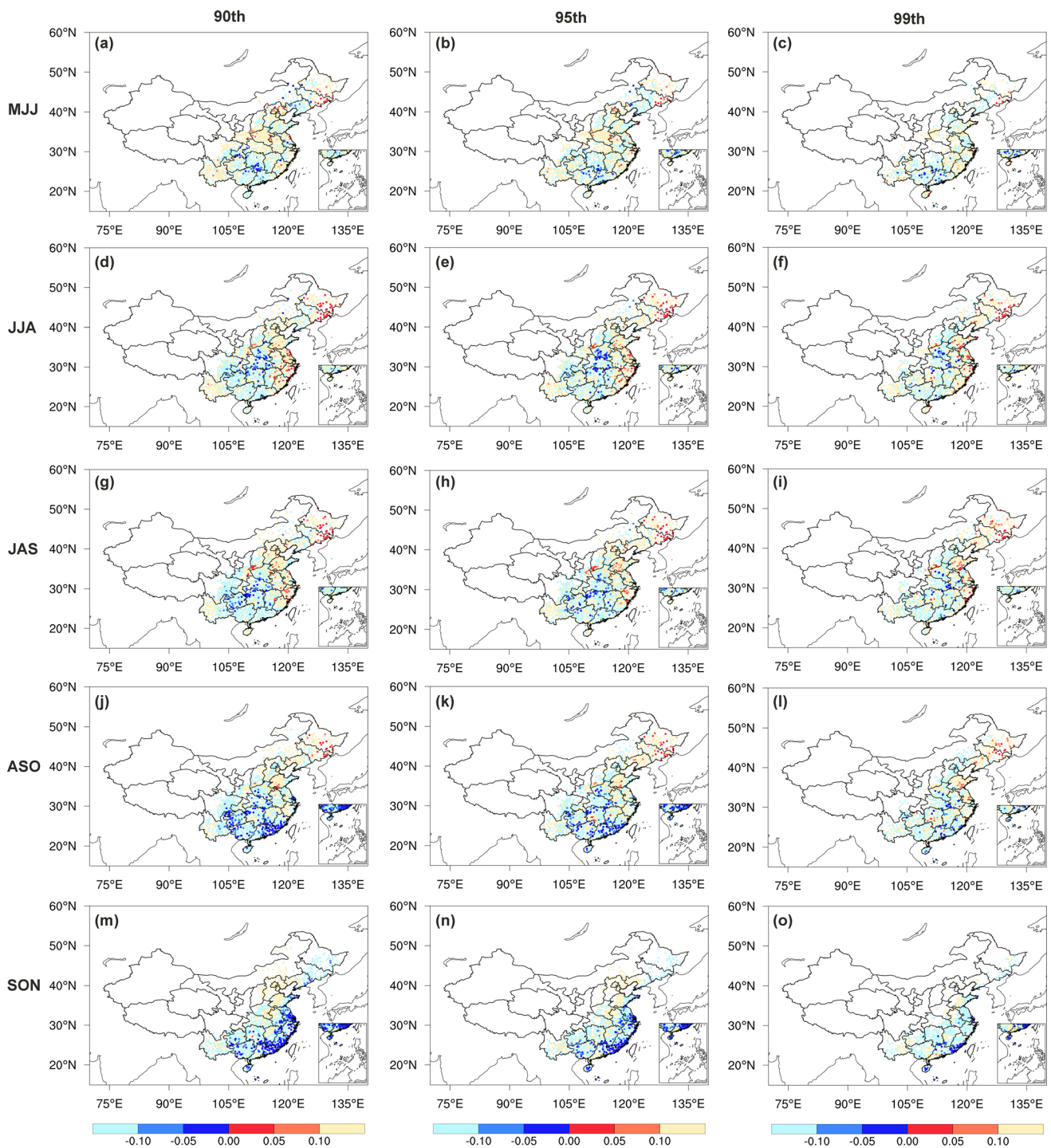


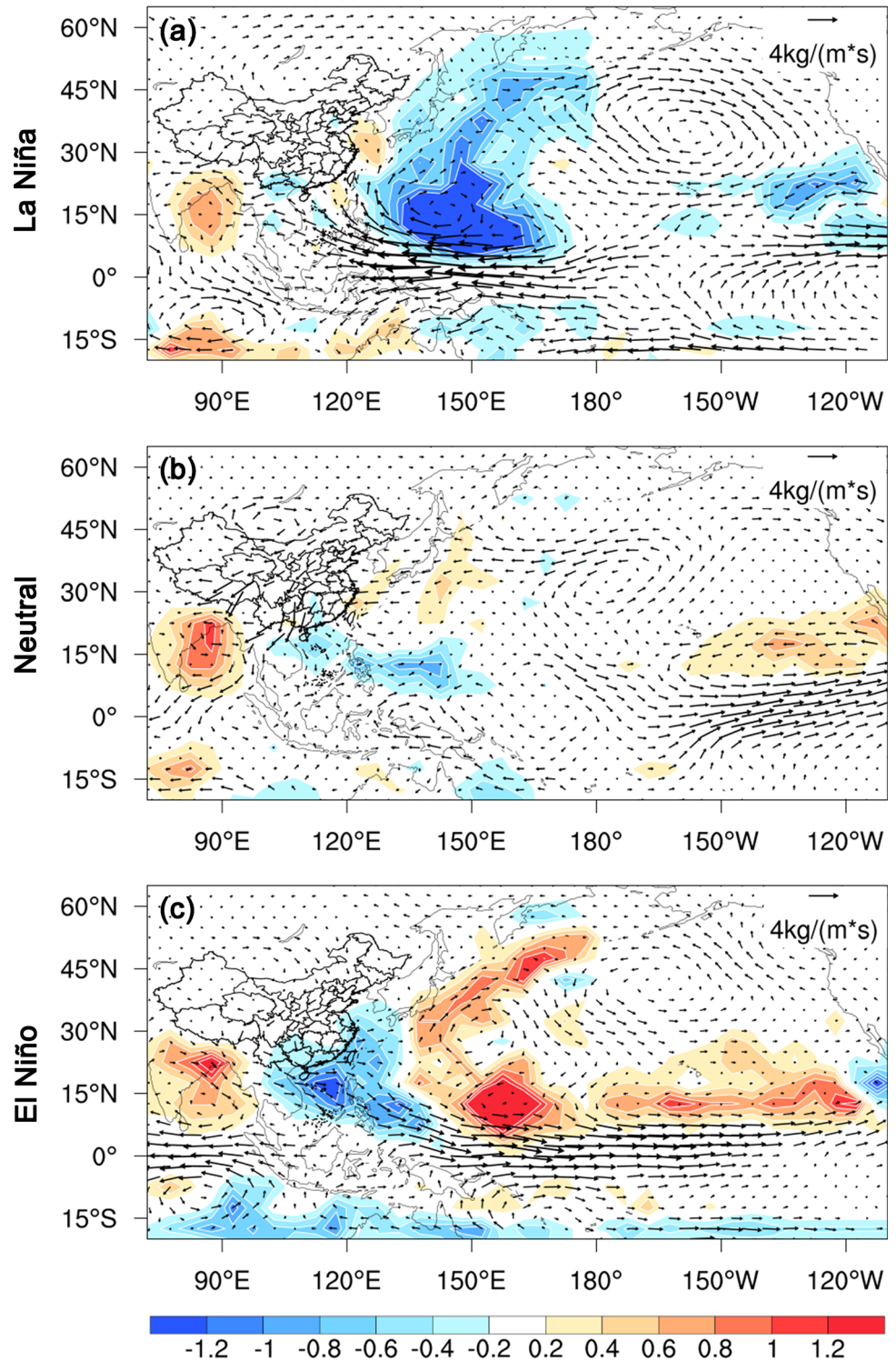
Fig. 8 Relationship between the frequency of tropical cyclone (TC)-induced extreme precipitation obtained by peak-over-threshold (POT) sampling and seasonal Niño-3.4 values in the mainland of China. The relationship was identified based on Poisson regression, and the colors are p values of the β_1 coefficients. Negative p values (blue circles) represent that the β_1 coefficients are less than zero, indicating a

greater probability of TC-induced POT precipitation during La Niña years, and positive p values (red circles) indicate a greater probability during El Niño years. The monthly Niño-3.4 values were averaged for each TC season: May–July (MJJ); June–August (JJA); July–September (JAS); August–October (ASO); and September–November (SON)

with westerly steering flow implies lower TC track density during an El Niño phase. For southeastern China, the evidently low TC track density can be attributed to the

prevalent westerly steering flow as well as the negative TC genesis anomalies over this region (Figs. 9c and 10c). The easterly steering flow from the Yellow Sea is beneficial for

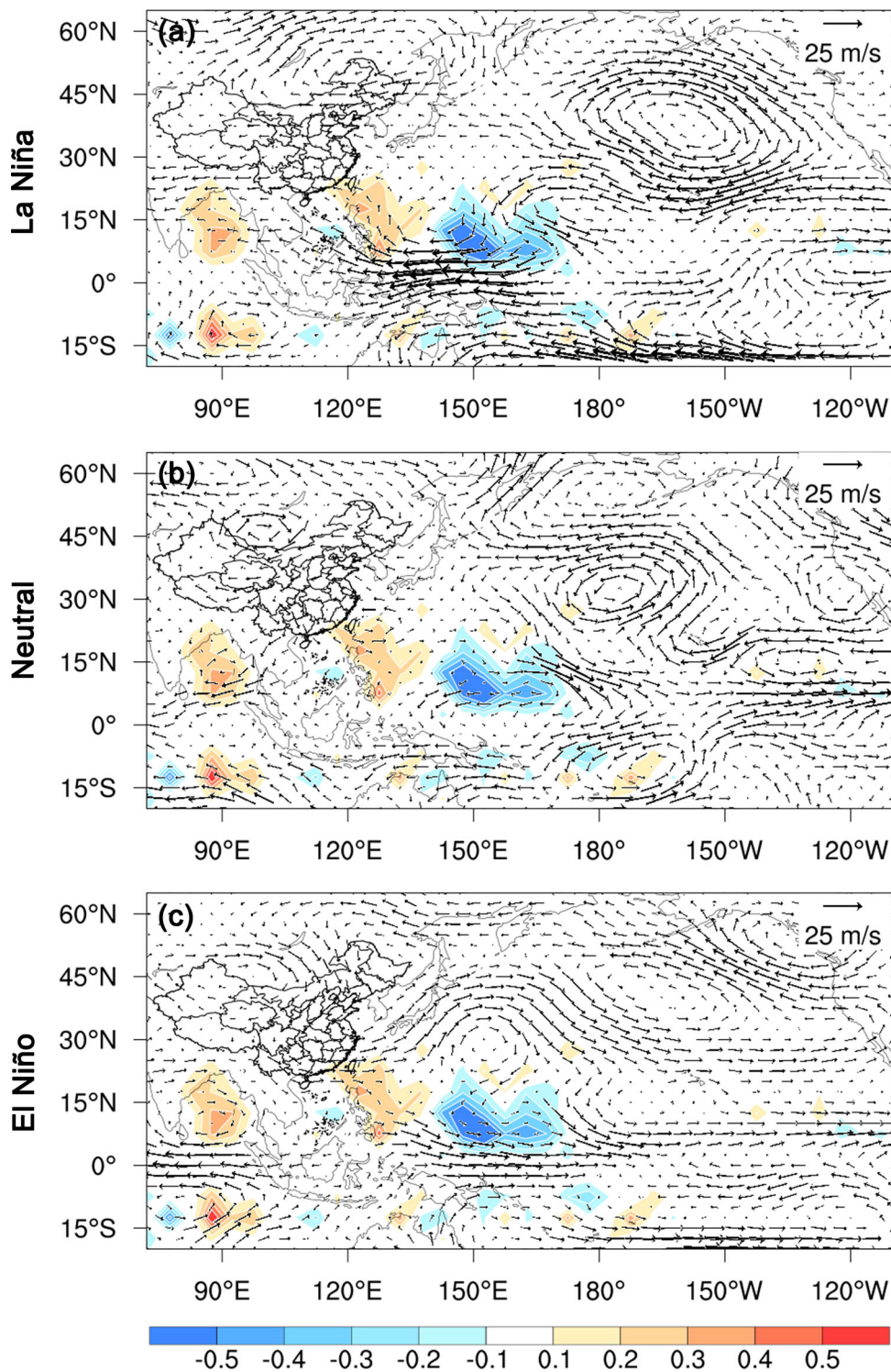
Fig. 9 Composited moisture flux ($\text{g}/\text{m}^2/\text{s}$) anomalies (arrows) and tropical cyclone (TC) track density anomalies (shadow) during La Niña phase (a), neutral phase (b), and El Niño phase (c). TC track density was calculated by binning the longitude and latitude of TC locations into $5^\circ \times 5^\circ$ grids



higher TC track density in the north and northeast China during La Niña years (Fig. 10). The WNP produces more TCs in La Niña years and more TCs that recurve toward the north and northeast, which leads to more extreme precipitation events in north and northeast China (Fig. 10a).

The large-scale environment of TC activity, such as SST, vorticity, divergence, and zonal wind, modulates TC growth and the source region of TC genesis (Tippett et al. 2011; Corporal-Lodangco et al. 2016; Zhang, Lai et al. 2018) (Fig. 11). We first calculated the anomalies of these large-scale environmental variables by extracting the

Fig. 10 Compositing steering flow (m/s) anomalies (arrows) and tropical cyclone (TC) genesis anomalies (shadow) during La Niña phase (a), neutral phase (b), and El Niño phase (c). TC genesis density is calculated by binning the longitude and latitude of TC locations into $5^\circ \times 5^\circ$ grids



difference relative to the means of these variables over 1961–1990. The average of a variable over a 30-year period is usually used to calculate the anomalies of this variable (Corporal-Lodangco et al. 2016; Gu et al. 2019a). Then, taking SST as an example, the composited anomalies during La Niña phase, neutral phase, and El Niño phase are

the averaged SST anomalies in the identified La Niña years, neutral years, and El Niño years, respectively. We also employed the *t* test method to detect whether there is a statistical discrepancy of the means between the two groups of samples (that is, anomalies in one ENSO phase and in 1961–1990). The *t*-test method can be used when the

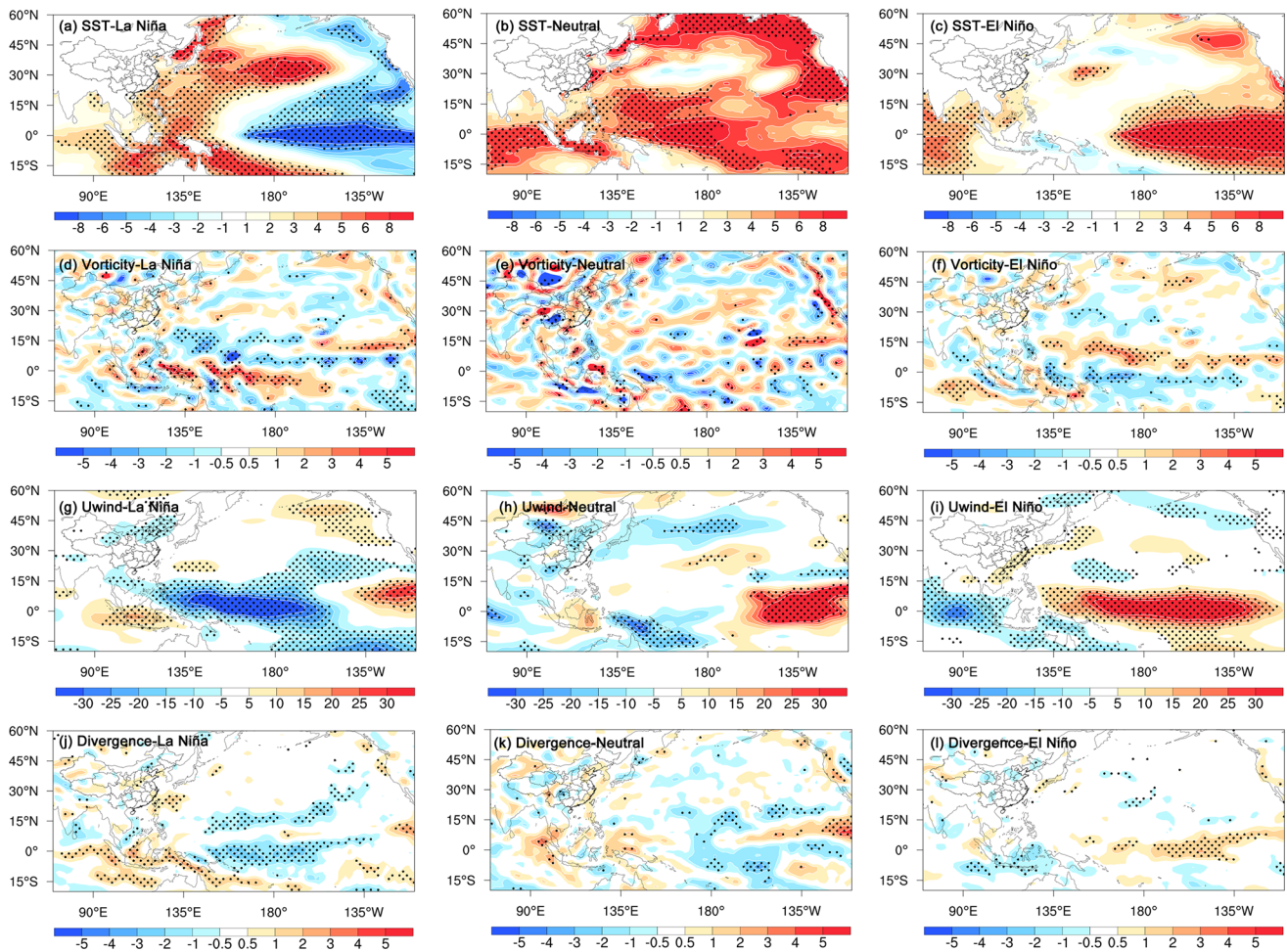


Fig. 11 Composited SST anomalies during La Niña phase (a), neutral phase (b), and El Niño phase (c), as well as low-level vorticity (1000-hPa) anomalies (d)–(f), zonal wind (850 hPa) anomalies (g)–

(i), and high-level vorticity (250 hPa) anomalies (j)–(l). The stippling indicates different significance at the 95% confident level

sample is normally distributed and its length is smaller than 30. The SST has a significant effect on the seasonal distribution of TC genesis location and frequencies (Shapiro and Goldenberg 1998; Corporal-Lodangco et al. 2016; Zhang, Lai et al. 2018). The central equatorial Pacific is the region where most of the WNP TCs are born (Mendelsohn et al. 2012). The SST anomalies are more pronouncedly positive during El Niño over the CEEP (central and eastern equatorial Pacific) (Figs. 11a–11c), which implies that the location of TCs genesis is likely to displace toward the east and southeast during El Niño years. Warmer SST is found over the WNP and is closer to China in La Niña years compared with El Niño years, which is related to the northwest movement of the origin of TCs. Therefore, La Niña years are more likely to witness TC-induced extreme precipitation over China. Variation in the atmospheric circulation related to ENSO alters the monsoon trough location, modifying TC genesis, intensities, and storm tracks (Frank 1987; Huangfu et al. 2017; Zhang, Lai et al.

2018). The increasing low-level vorticity and upper-level divergence that strengthen an atmospheric disturbance also benefit TC genesis. In the CEEP, we can observe a stronger 1000-hPa vorticity during an El Niño phase (Figs. 11d–11f). Simultaneously, the CEEP also shows evident positive upper-level (250 hPa) divergence anomalies only during El Niño phases (Figs. 11i–j), which could promote the development of surface low pressure areas (Corporal-Lodangco et al. 2016a, b; Zhang, Lai et al. 2018). Compared with the La Niña and neutral phases, the strong positive zonal wind anomalies in the CEEP during an El Niño phase indicate that the westerlies are prevalent over this region (Figs. 11g–i). The prevalent westerlies could push the warm pool eastward and displace the origin location of TC eastward as well. Under these conditions, the number of landfall TCs over China is likely to reduce during El Niño phases. In summary, during an El Niño phase, higher SST, heavier low-level vorticity, and upper-level divergence over the CEEP lead to fewer TCs being

produced and displace the genesis locations of TCs eastward at which point the prevalent westerlies push TCs far away from China. The distribution of meteorological factors makes a significant contribution to extreme precipitation over China caused by TCs during El Niño phases (Corporal-Lodangco et al. 2016; Zhang, Lai et al. 2018). These results are consistent with the evidently negative TC track density anomalies over southeastern China (Fig. 9c).

5 Conclusion

We examined the connections between the WNP TCs and extreme precipitation over China based on daily precipitation measurements from 1960 to 2016 at 1937 stations. The AM and POT methods were used to extract the magnitude and frequency of extreme precipitation from daily observations. The contributions of TCs to extreme precipitation highlight that TCs play a significant role in causing precipitation extremes in eastern China with a natural line divided by the undulating mountains—the Great Khingan-Taihang-Wushan-Xuefeng Mountain). Tropical cyclone-induced extreme precipitation accounts for more than 50% of the total extreme precipitation events in the southeast coast of China. The contributions are independent of the durations of AM precipitation (1–3 days), but increase evidently in more extreme POT precipitation defined by higher thresholds. However, most stations in China do not show significance variation in the TC-induced extreme precipitation over the most recent 57 years.

The logistic and Poisson regressions were employed to explore the role of ENSO in regulating the likelihood of AM extremes and the frequency of POT events, respectively. We found that El Niño (La Niña) years witness a decreased (increased) likelihood of TC-induced precipitation extremes in southeastern China where initial TC landfall typically occurs, as well as in northern and northeastern China, which are impacted by the recurring trajectories of many TCs that become controlled by the Westerlies in their latter stages. The signals are stronger in POT events than AM events, indicating that ENSO is likely to witness a stronger regulation on the frequency of TC-induced extreme precipitation.

The relationship between TC-induced extreme precipitation and ENSO can be readily explained by the responses of TC tracks to ENSO. Southeastern China is assaulted by fewer TCs during El Niño phases, which is attributed to the prevalent westerly steering flow over this region. The integrated vapor transport is abnormally transited from northern to southern China during the El Niño years, which is not favorable to provide sufficient moisture flux for TC-induced extreme precipitation. The CEEP—the major TCs formation region—shows warmer SSTs, larger vorticity

and divergence, and more vigorous westerlies during El Niño years, which produce fewer TCs and displace the mean genesis locations of TCs far from China (Corporal-Lodangco et al. 2016; Zhang, Lai et al. 2018).

Our results show that TC-induced extreme precipitation over China is significantly modulated by ENSO and this modulation depends on regions. Although it is a huge challenge to predict the TC generation time and track and intensity, the multiple month advance prediction of ENSO is possible through statistical methods and/or numerical simulation models (Chen et al. 2020; Glantz and Ramirez 2020; Yan et al. 2020). Combining our results and the prediction of ENSO can provide a reference for decision makers on whether southeastern (northern and northeastern) China may face a greater risk of TC-induced extreme precipitation in the next few months, and adaptation measures can be taken to mitigate the possible hazard induced by TCs.

Acknowledgements This work was financially supported by the Open Research Fund of the State Key Laboratory of Simulation and Regulation of Water Cycle in River Basin (China Institute of Water Resources and Hydropower Research, Grant No. IWHR-SKL-201919), the National Key Research and Development Program of China (Grant No. 2018YFA0605603), the National Natural Science Foundation of China (Grant Nos. 41901041 and U1911205), the Fundamental Research Funds for the Central Universities, China University of Geosciences (Wuhan) (Grant No. 2020G12). We thank the International Best Track Archive for Climate Stewardship for providing access to its archive of TC data, and the Climate Prediction Center of the National Oceanic and Atmospheric Administration (NOAA) for access to the monthly ENSO data. The data used to analyze the dynamic mechanisms were obtained from the National Centers for Environmental Prediction (NCEP)-National Center for Atmospheric Research (NCAR) reanalysis dataset. We gratefully acknowledge the help of China Meteorological Administration staff in accessing meteorological data and the help of Data Center for Resources and Environmental Sciences, Chinese Academy of Sciences in accessing digital elevation model data at <http://www.resdc.cn>.

Open Access This article is licensed under a Creative Commons Attribution 4.0 International License, which permits use, sharing, adaptation, distribution and reproduction in any medium or format, as long as you give appropriate credit to the original author(s) and the source, provide a link to the Creative Commons licence, and indicate if changes were made. The images or other third party material in this article are included in the article's Creative Commons licence, unless indicated otherwise in a credit line to the material. If material is not included in the article's Creative Commons licence and your intended use is not permitted by statutory regulation or exceeds the permitted use, you will need to obtain permission directly from the copyright holder. To view a copy of this licence, visit <http://creativecommons.org/licenses/by/4.0/>.

References

- Aryal, Y.N., G. Villarini, W. Zhang, and G.A. Vecchi. 2018. Long term changes in flooding and heavy rainfall associated with

- North Atlantic tropical cyclones: Roles of the North Atlantic Oscillation and El Niño-Southern Oscillation. *Journal of Hydrology* 559: 698–710.
- Camargo, S.L., and A.H. Sobel. 2005. Western North Pacific tropical cyclone intensity and ENSO. *Journal of Climate* 18(15): 2996–3006.
- Chan, J.C.L. 2000. Tropical cyclone activity over the western North Pacific associated with El Niño and La Niña events. *Journal of Climate*, 13(16): 2960–2972.
- Chan, J.C.L., and W.M. Gray. 1982. Tropical cyclone movement and surrounding flow relationships. *Monthly Weather Review* 110(10): 1354–1374.
- Chan, J.C.L., and W. Zhou. 2005. PDO, ENSO and the early summer monsoon rainfall over south China. *Geophysical Research Letters* 32(8): Article L08810.
- Chang, C.-P., Y. Lei, C.-H. Sui, X. Lin, and F. Ren. 2012. Tropical cyclone and extreme rainfall trends in East Asian summer monsoon since mid-20th century. *Geophysical Research Letters* 39: Article L18702.
- Chen, J.-M., T. Li, C.-F. Shih. 2010. Tropical cyclone- and monsoon-induced rainfall variability in Taiwan. *Journal of Climate* 23(15): 4107–4120.
- Chen, X., L. Wu, and J. Zhang. 2011. Increasing duration of tropical cyclones over China. *Geophysical Research Letters* 38: Article L02708.
- Chen, H.-C., Y.-H. Tseng, Z.-Z. Hu, and R. Ding. 2020. Enhancing the ENSO predictability beyond the spring barrier. *Scientific Reports* 10(1): 1–12.
- Corporal-Lodangco, I.L., L.M. Leslie, and P.J. Lamb. 2016. Impacts of ENSO on Philippine tropical cyclone activity. *Journal of Climate* 29(5): 1877–1897.
- Frank, W.M. 1987. Tropical cyclone formation. In *A global view of tropical cyclones*, ed. R.L. Elsberry, 53–90. Arlington, VA: Office of Naval Research.
- George, J.E., and W.M. Gray. 1976. Tropical cyclone motion and surrounding parameter relationships. *Journal of Applied Meteorology* 15(12): 1252–1264.
- Glantz, M.H., and I.J. Ramirez. Reviewing the Oceanic Niño Index (ONI) to enhance societal readiness for El Niño's impacts. *International Journal of Disaster Risk Science* 11(3). <https://doi.org/10.1007/s13753-020-00275-w>.
- Gu, X., Q. Zhang, V.P. Singh, and P. Shi. 2017a. Changes in magnitude and frequency of heavy precipitation across China and its potential links to summer temperature. *Journal of Hydrology* 547: 718–731.
- Gu, X., Q. Zhang, V.P. Singh, and P. Shi. 2017b. Non-stationarities in the occurrence rate of heavy precipitation across China and its relationship to climate teleconnection patterns. *International Journal of Climatology* 37(11): 4186–4198.
- Gu, X., Q. Zhang, V.P. Singh, L. Liu, and P. Shi. 2017c. Spatiotemporal patterns of annual and seasonal precipitation extreme distributions across China and potential impact of tropical cyclones. *International Journal of Climatology* 37(10): 3949–3962.
- Gu, X., Q. Zhang, J. Li, V.P. Singh, J. Liu, P. Sun, and C. Cheng. 2019a. Attribution of global soil moisture drying to human activities: A quantitative viewpoint. *Geophysical Research Letters* 46(5): 2573–2582.
- Gu, X., Q. Zhang, V.P. Singh, C. Song, P. Sun, and J. Li. 2019b. Potential contributions of climate change and urbanization to precipitation trends across China at national, regional and local scales. *International Journal of Climatology* 39(6): 2998–3012.
- Gu, X., Q. Zhang, J. Li, L. Liu, C. Xu, and P. Sun. 2020. The changing nature and projection of floods across Australia. *Journal of Hydrology* 584: Article 124703.
- Huangfu, J., R. Huang, W. Chen, T. Feng, and L. Wu. 2017. Interdecadal variation of tropical cyclone genesis and its relationship to the monsoon trough over the western North Pacific. *International Journal of Climatology* 37(9): 3587–3596.
- Jiang, H., and E.J. Zipser. 2010. Contribution of tropical cyclones to the global precipitation from eight seasons of TRMM data: Regional, seasonal, and interannual variations. *Journal of Climate* 23(6): 1526–1542.
- Jiang, M., and L. Qi. 2016. Analysis on climate characteristics of extreme precipitation typhoon in China during 1959–2012. *Meteorological Monthly* 42(10): 1230–1236 (in Chinese).
- Jonkman, S.N., B. Maaskant, E. Boyd, and M.L. Levitan. 2009. Loss of life caused by the flooding of New Orleans after Hurricane Katrina: Analysis of the relationship between flood characteristics and mortality. *Risk Analysis* 29(5): 676–698.
- Kendall, M.G. 1975. *Rank correlation methods*. London: Charles Griffin.
- Khouakhi, A., and G. Villarini. 2017. Attribution of annual maximum sea levels to tropical cyclones at the global scale. *International Journal of Climatology* 37(1): 540–547.
- Khouakhi, A., G. Villarini, and G. Vecchi. 2017. Contribution of tropical cyclones to rainfall at the global scale. *Journal of Climate* 30(1): 359–372.
- Knapp, K.R., M.C. Kruk, D.H. Levinson, H.J. Diamond, and C.J. Neumann. 2010. The International Best Track Archive for Climate Stewardship (IBTrACS): Unifying tropical cyclone data. *Bulletin of the American Meteorological Society* 91(3): 363–376.
- Knight, D.B., and R.E. Davis. 2009. Contribution of tropical cyclones to extreme rainfall events in the southeastern United States. *Journal of Geophysical Research* 114: Article D23102.
- Krishnamurthy, L., G. Vecchi, R. Msadek, H. Murakami, A. Wittenberg, and F. Zeng. 2016. Impact of strong ENSO on regional tropical cyclone activity in a high-resolution climate model in the North Pacific and North Atlantic Oceans. *Journal of Climate* 29(7): 2375–2394.
- Lee, M.-H., C.-H. Ho, and J.-H. Kim. 2010. Influence of tropical cyclones landfalls on spatiotemporal variations in typhoon season rainfall over South China. *Advances in Atmospheric Sciences* 27(2): 443–454.
- Lyon, B., and S.J. Camargo. 2009. The seasonally-varying influence of ENSO on rainfall and tropical cyclone activity in the Philippines. *Climate Dynamics* 32(1): 125–141.
- Ma, F., X. Yuan, and A. Ye. 2015. Seasonal drought predictability and forecast skill over China. *Journal of Geophysical Research* 120(16): 8264–8275.
- Mann, H.B. 1945. Nonparametric tests against trend. *Econometrica* 13(3): 245–259.
- Mendelsohn, R., K. Emanuel, S. Chonabayashi, and L. Bakkensen. 2012. The impact of climate change on global tropical cyclone damage. *Nature Climate Change* 2(3): 205–209.
- Mumby, P.J., R. Vitolo, and D.B. Stephenson. 2011. Temporal clustering of tropical cyclones and its ecosystem impacts. *Proceedings of the National Academy of Sciences of the United States of America* 108(43): 17626–17630.
- Nayak, M.A., G. Villarini, and A. Bradley. 2016. Atmospheric rivers and rainfall during NASA's Iowa flood studies (IFloodS) campaign. *Journal of Hydrometeorology* 17(1): 257–271.
- Peduzzi, P., B. Chatenoux, H. Dao, A.D. Bono, C. Herold, J. Kossin, F. Mouton, and O. Nordbeck. 2012. Global trends in tropical cyclone risk. *Nature Climate Change* 2(4): 289–294.
- Ren, F., Y. Wang, X. Wang, and W. Li. 2007. Estimating tropical cyclone precipitation station observation. *Advances in Atmospheric Sciences* 24(4): 700–711.

- Ren, F., G. Wu, W. Dong, X. Wang, Y. Wang, W. Ai, and W. Li. 2006. Changes in tropical cyclone precipitation over China. *Geophysical Research Letters* 33(20): Article L20702.
- Shapiro, L.J., and S.B. Goldenberg. 1998. Atlantic sea surface temperatures and tropical cyclone formation. *Journal of Climate* 11(4): 578–590.
- Shepherd, M.J., A. Grundstein, and T.L. Mote. 2007. Quantifying the contribution of tropical cyclones to extreme rainfall along the coastal southeastern United States. *Geophysical Research Letters* 34(23): Article L23810.
- Smith, J.A., G. Villarini, and M.L. Baeck. 2011. Mixture distributions and the hydroclimatology of extreme rainfall and flooding in the eastern United States. *Journal of Hydrometeorology* 12(2): 294–308.
- Teegavarapu, R.S.V. 2013. *Floods in a changing climate: Extreme precipitation*. Cambridge: Cambridge University Press.
- Tippett, M.K., S.J. Camargo, and A.H. Sobel. 2011. A Poisson regression index for tropical cyclone genesis and the role of large-scale vorticity in genesis. *Journal of Climate* 24(9): 2335–2357.
- Vellore, R.K., M. L. Kaplan, P. Krishnan, et al. 2016. Monsoon-extratropical circulation interactions in Himalayan extreme rainfall. *Climate Dynamics* 46(11–12): 3517–3546.
- Villarini, G., and R.F. Denniston. 2016. Contribution of tropical cyclones to extreme rainfall in Australia. *International Journal of Climatology* 36(2): 1019–1025.
- Villarini, G., R. Goska, J.A. Smith, and G.A. Vecchi. 2014. North Atlantic tropical cyclones and U.S. flooding. *Bulletin of the American Meteorological Society* 95(9): 1381–1388.
- Villarini, G., J.A. Smith, and G.A. Vecchi. 2013. Changing frequency of heavy rainfall over the central United States. *Journal of Climate* 26(1): 343–350.
- Wang, B., and J.C.L. Chan. 2002. How strong ENSO events affect tropical storm activity over the western North Pacific. *Journal of Climate* 15(13): 1643–1658.
- Wang, L., H. Behling, S. Kao, H. Li, K. Selvaraj, M. Hsieh, Y. Chang. 2015. Late Holocene environment of subalpine northeastern Taiwan from pollen and diatom analysis of lake sediments. *Journal of Asian Earth Sciences* 114: 447–456.
- Webster, P.J., H.J. Holland, J.A. Curry, and H.R. Chang. 2005. Changes in tropical cyclone number, duration, and intensity in a warming environment. *Science* 309(5742): 1844–1846.
- Wu, R.G., Z.Z. Hu, and B.P. Kirtman. 2003. Evolution of ENSO-related rainfall anomalies in East Asia. *Journal of Climate* 16(22): 3742–3758.
- Yan, J., L. Mu, L. Wang, R. Ranjan, and A.Y. Zomaya. 2020. Temporal convolutional networks for the advance prediction of ENSO. *Scientific Reports* 10: Article 8055.
- Yang, L., M. Liu, J.A. Smith, and F. Tian. 2017. Typhoon Nina and the August 1975 flood over Central China. *Journal of Hydrometeorology* 18(2): 451–472.
- Yin, Y., M. Gemmer, Y. Luo, and Y. Wang. 2010. Tropical cyclones and heavy rainfall in Fujian Province, China. *Quaternary International* 226(1–2): 122–128.
- Zhang, Q., X. Gu, J. Li, P. Shi, and V.P. Singh. 2018. The impact of tropical cyclones on extreme precipitation over coastal and inland areas of China and its association to ENSO. *Journal of Climate* 31(5): 1865–1880.
- Zhang, Q., Y. Lai, X. Gu, P. Shi, and V.P. Singh. 2018. Tropical cyclonic rainfall in China: Changing properties, seasonality, and causes. *Journal of Geophysical Research* 123(9): 4476–4489.
- Zhang, Q., Q. Liu, and L. Wu. 2009. Tropical cyclone damages in China 1983–2006. *Bulletin of the American Meteorological Society* 90(4): 489–495.
- Zhang, Q., V.P. Singh, J. Li, and X. Chen. 2011. Analysis of the periods of maximum consecutive wet days in China. *Journal of Geophysical Research* 116: Article D23106.
- Zhang, Q., Y. Wang, V.P. Singh, X. Gu, D. Kong, and M. Xiao. 2016. Impacts of ENSO and ENSO Modoki + A regimes on seasonal precipitation variations and possible underlying causes in the Huai River basin, China. *Journal of Hydrology* 533: 308–319.
- Zhou, W., C.Y. Li, and J.C.L. Chan. 2006. The interdecadal variations of the summer monsoon rainfall over South China. *Meteorology and Atmospheric Physics* 93(3–4): 165–175.